MOLECULAR MACHINES

A molecular anion pump

Baihao Shao†‡, Heyifei Fu†, Ivan Aprahamian*

Pumping ions against a concentration gradient through protein-based transporters is a cornerstone of numerous biological processes. Mimicking this function by using artificial receptors remains a daunting challenge, mainly because of the difficulties in balancing between the requirement for high binding affinities and precise and on-demand ion capture and release properties. We report a trimeric hydrazone photoswitch-based receptor that converts light energy into work by actively transporting chloride anion against a gradient through a dichloromethane liquid membrane, functioning as a molecular pump. The system manifests ease of synthesis, bistability, excellent photoswitching properties, and superb ON-OFF binding properties (difference of up to six orders of magnitude).

Ion pumps, which are biological machines that actively transport ions across a membrane against a gradient, play a crucial role in regulating biological processes (*1*). For example, the Na-K-Cl cotransporter (*2*), which is ubiquitously distributed across various tissues and cell types all over the human body, has a crucial function in regulating electrolyte balance (*3*), blood pressure (*4*), cell volume (*5*), tubular reabsorption (*6*), and early neuronal development (*7*). Mimicking such biological transporters, especially ones that transport anions, has huge societal benefits because such systems can be used in, for example, the remediation of water from pollutants (*8*) such as radioactive elements from nuclear waste (*9*). Although several beautiful molecular pumps (*10*–*13*), all based on interlocked systems (*14*), have been designed and developed in recent years, they have yet to be used in active ion or anion transport (*15*). An appealing approach to accomplishing such a goal is the use of synthetic anion receptors (*16*–*19*), such as amides, squaramides, ureas, thioureas, triazoles, and calixpyrroles (*20*), as well as halogen and chalcogen bonds (*21*). Moreover, and to result in active anion transport, the binding capability of such receptors needs to be externally modulated. If successful, such systems will be able to move anions against a gradient while consuming energy—functioning as molecular anion pumps. In general, the combination of a photochromic compound, such as stilbenes (*22*) and azobenzenes (*23*, *24*), with anion receptors introduces photoresponsive functionality to the latter through the light-controlled modulation of supramolecular (such as halogen bonding, cation–anion-π interactions, and H bonding) interactions (*25*–*27*) or altering the cooperativity between binding units (*28*). This intricate interplay of molecular design and light manipulation can in principle pave the way for the development of advanced supramolecular ion pumps and machines. Such an approach has resulted in limited examples of active artificial proton and cation (Ca^{2+}) transporters (*29*–*31*). However, anion recognition is more challenging (*32*), and moving anions against a gradient is a daunting task because it entails among other things the development of anion-recognition motifs that can be efficiently turned ON and OFF with light. In this vein, Flood and coworkers, who pioneered the use of CH bonds in anion recognition (*33*), developed azobenzene-based foldamers that exhibit light-induced chloride (Cl^-) capture and release, leveraging a 10-fold difference between the two isomerization states to produce current changes (*23*). Kerckhoffs and Langton have used azobenzene in conjunction with squaramides to facilitate Cl^- transport across membranes as well (*34*). Another approach by Busschaert *et al.* (*35*) and Wezenberg *et al.* (*36*) involves the use of stilbene-based photoswitches, coupled with bis-thioureas to realize Cl^- uniport selectivity across a membrane. More recently, the latter group developed a stilbene-strapped calix[4]pyrrole, an anion recognition motif developed by Kim and Sessler (*37*) that demonstrated a record change of four orders of magnitude in Cl^- binding upon photoisomerization (*28*). However, the use of such synthetic receptors has so far been limited to passive transport, therefore only allowing for the diffusion of anions down a concentration gradient (equilibration). This outcome is reminiscent of the pioneering U-tube experiments by Shinkai *et al.*, in which cations were also transported down a gradient (*38*). These results can be mainly attributed to the inherent limitations of the photochromic units used in such applications. For example, and in the case of azobenzene (*23*, *24*, *34*, *38*), its fast thermal back isomerization [thermal half-life ($\tau_{1/2}$)] prevents optimal binding for extended periods of time, and its low quantum yields and photostationary states (PSSs) limit the amount of anions that can be transported even if the photoinduced ON/OFF ratios are high. Obtaining high ratios is in general difficult because the anion receptor and photoswitch are usually separate units, which makes it challenging to optimize their congruent operation. Such limitations have been overall a major hurdle in the use of photoswitchable receptors in active anion transport and hence their use in developing anion concentration gradients across membranes (*17*). Recently, the photoinduced asymmetric surface charge redistribution (holes are produced at the illumination side, while electrons migrate away from it) in a porphyrin-containing polymer membrane has been used in Cl^- pumping (*39*). Under illumination, the Cl^- ions are enriched at the positively charged side of the polymer while being repelled from the opposite side, which results in a localized concentration gradient that is responsible for the anion transport. This design, which relies on bulk effects (is not molecular in function), yields a fast (minutes timescale) and efficient (for example, the light to electric energy conversion efficiency is ~0.27%) pumping operation.

Hydrazones (*40*, *41*) are emerging as photochromes of choice in addressing many of the drawbacks associated with legacy photoswitches such as azobenzenes and stilbenes, which have stymied progress in many fields, including ion transport. Of interest is the acidic nature of the NH bond, which has been previously used in anion (particularly fluoride) sensing (*40*, *42*). This bond is also part of the core structural motif of a bistable hydrazone (extrapolated $\tau_{1/2}$ of up to 5000 years) in its *Z* form, the central H-bonded six-membered ring (Fig. 1A). Upon photoisomerization to the *E* isomer, this H bond is disrupted. This structural change and acidity of the NH bond inspired us to design a trimeric hydrazone receptor **1** (Fig. 1, B and C) with three polarized hydrazone N–H bonds that can be photoswitched on demand to either disengage from the environment (*Z* form) or engage with it (associate with anions in the *E* form). We hypothesized that having the photoswitch also function as the anion receptor would result in enhanced ON/OFF binding capabilities. Moreover, we opted to use the *para*-NO_2 derivative of the hydrazone because it enhances the isomerization efficiency (for example, high PSS) and further polarizes the N–H bond to bind more strongly with anions (*43*). Using this strategy, we were able to show that the *E* isomer of **1** binds more strongly (Table 1) to halogen anions (Cl^-, Br^-, and I^-) in dichloromethane (DCM) and less so with larger anions (BF_4^- and PF_6^-). By contrast, the *Z* isomer shows minimal binding with the anions considering that all NH bonds are disengaged from the environment because of the intramolecular H bond. This difference in binding affinity resulted in the highly efficient

Department of Chemistry, Dartmouth College, Hanover, NH 03755, USA.
*Corresponding author. Email: ivan.aprahamian@dartmouth.edu
†These authors contributed equally to this work.
‡Present address: Department of Physiology, Anatomy and Genetics and Kavli Institute for Nanoscience Discovery, University of Oxford, Oxford OX1 3QU, UK.

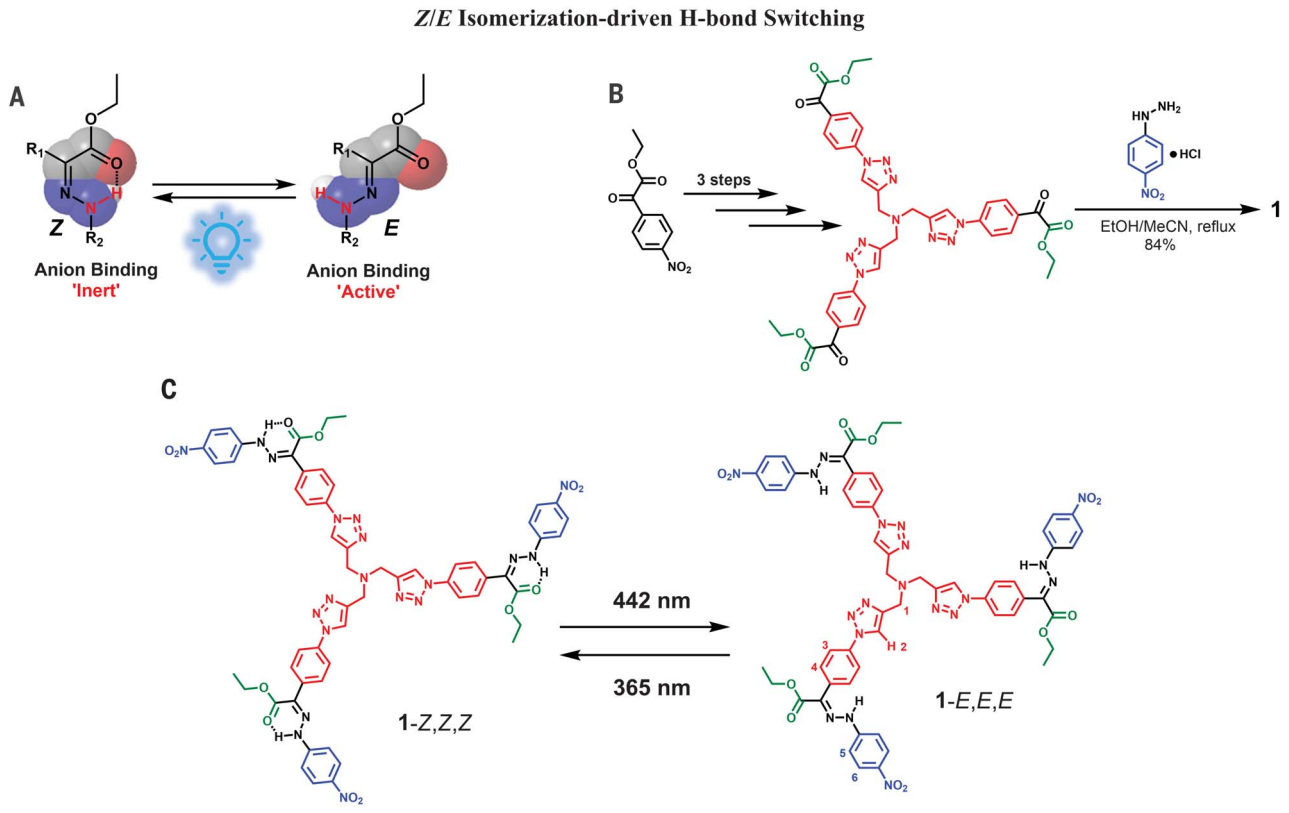

Fig. 1. Synthesis and structure of the trimeric hydrazone. (**A**) Core structural motif of the bistable hydrazones showing how photoisomerization results in turning the H-bonding motif ON and OFF. (**B**) Straightforward synthesis of the trimeric hydrazone receptor **1**. Et, ethyl; Me, methyl. (**C**) Photoisomerization process converting the nonbinding trimer **1**-*Z,Z,Z* to the anion receptor **1**-*E,E,E* by using 442- and 365-nm light irradiation.

photocapture and photorelease (difference of up to six orders of magnitude) of chloride ions by **1** in DCM. The effective photoisomerization (PSSs > 93%) and bistability ($\tau_{1/2}$ of years) of the receptor allowed us to actively pump potassium chloride (KCl) through a DCM liquid membrane embedded in a U-shaped tube. By doing so, we created an artificial molecular pump that consumes light energy to transport Cl^- against a concentration gradient, thus producing useful work (*44*).

Receptor synthesis

Compound **1** was synthesized in a straightforward manner with a 62% overall yield starting from the commercially available compound **5** (fig. S1). The intermediates and final product **1** were fully characterized by use of nuclear magnetic resonance (NMR) spectroscopy (figs. S2 to S15) and mass spectrometry. We next studied the photophysical and photochromic properties of **1** using ultraviolet/visible (UV/Vis) spectroscopy (Fig. 2A). **1**-*Z,Z,Z* shows an absorption maximum (λ_{max}) at 398 nm, with a molar absorption coefficient (ε) of 99,000 M^{-1} cm^{-1}. Upon irradiation with 442 nm [Andover bandpass filter 442F5X10-25 with a half bandwidth (HBW) of 10 nm and a transmission threshold of 75%] light (Fig. 1A), *Z*→*E* isomerization takes place to yield an *E*-rich PSS (PSS_{442}) that consists of 97% **1**-*E,E,E* isomer based on an extrapolation of the UV/Vis data (fig. S16) and proceeds with a quantum yield ($\Phi_{Z\rightarrow E}$) of 4.8 ± 0.1% (fig. S18). The pure absorption band of **1**-*E,E,E* (λ_{max} = 370 nm; ε = 86,000 M^{-1} cm^{-1}) was extrapolated (fig. S17) by following a previously reported method (*43*). Irradiation with 365-nm (Andover bandpass filter 365HC10-25 with an HBW of 10 nm and a transmission threshold of 90%) light triggers back isomerization and leads to a PSS_{365} consisting of 93% **1**-*Z,Z,Z*, with a quantum yield ($\Phi_{E\rightarrow Z}$) of 4.8 ± 0.5% (fig. S19) (*45*). Each hydrazone unit in the trimer isomerizes separately, resulting in an efficient *Z,Z,Z* to *E,E,E* transformation; hence, moving forward (and for simplicity), we will refer to this as a *Z*/*E* process. The

Table 1. Summary of the binding affinity of hydrazone 1 with the different anions.

Configuration	Anion†	Binding constant
1-*E,E,E**	Cl^-	2.05 ± 0.14 × 10^6 M^{-2}‡
	Br^-	1.48 ± 0.13 × 10^6 M^{-2}‡
	I^-	5.96 ± 0.48 × 10^5 M^{-2}‡
	BF_4^-	9.57 ± 0.59 × 10^2 M^{-1}§
	PF_6^-	6.50 ± 0.06 × 10^2 M^{-1}§
1-*Z,Z,Z*	Cl^-	9 ± 1 M^{-1}¶
	Br^-	7 ± 1 M^{-1}¶
	I^-	2 ± 1 M^{-1}¶

*__1__-*E,E,E* samples (97%) were obtained by irradiating **1** with the 442-nm light in CD_2Cl_2 until the PSS was reached. †Anions were introduced in the form of *t*-butylammonium salts (TBA^+X^-). ‡Binding constants were fit by using *HypNMR2008* based on a 2:1 model. §Binding constants were fit by using *HypNMR-2008* based on a 1:1 model. ¶Interactions were too weak to determine binding stoichiometry; binding constants were fit by using *HypNMR2008* based on a 1:1 model.

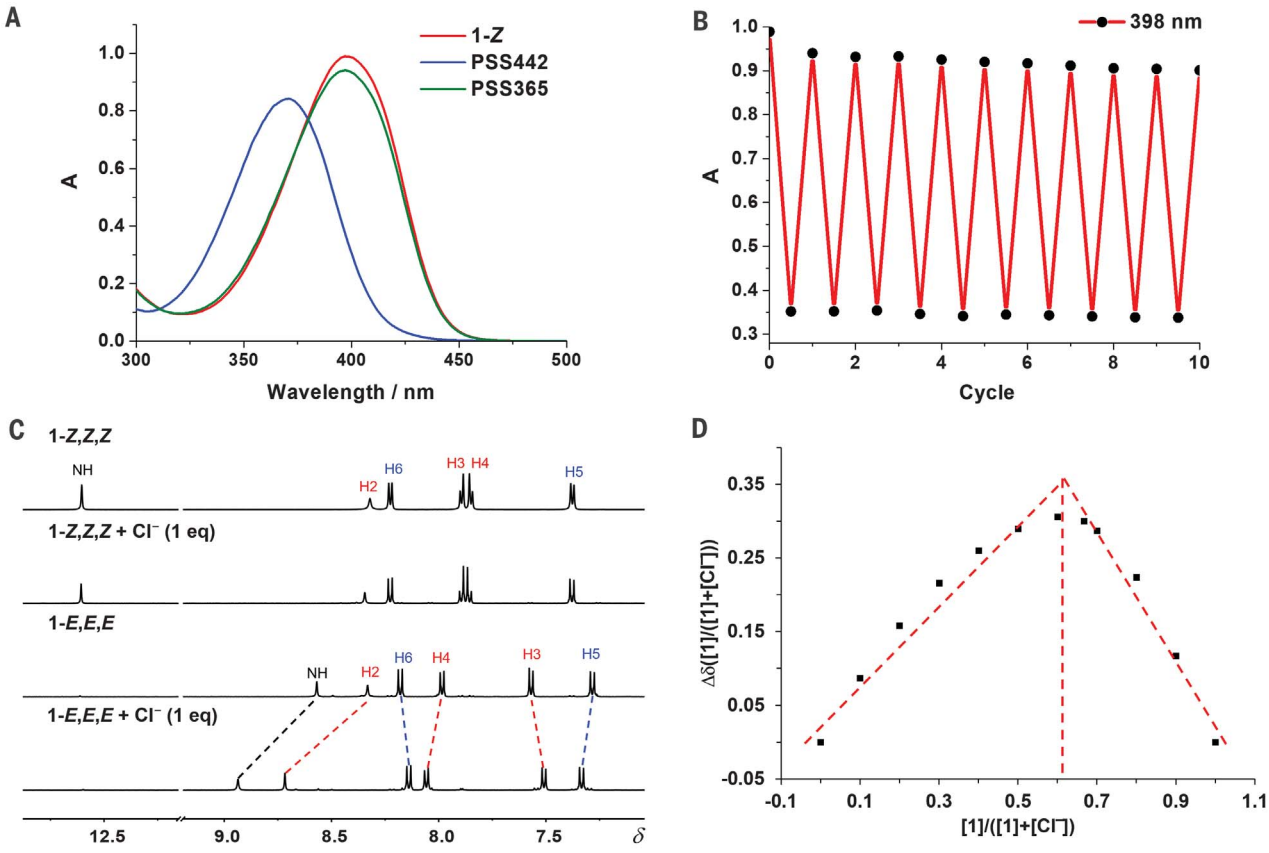

Fig. 2. The UV/Vis spectroscopy studies of the photoisomerization of hydrazone switch 1 in DCM and the binding analyses with Cl^- in CD_2Cl_2. (**A**) UV/Vis spectra (1×10^{-5} M) of pristine **1**-*Z*,*Z*,*Z* (red line) and at different PSSs (442 and 365 nm) in DCM. (**B**) Photoisomerization cycles of hydrazone **1** in DCM upon alternating the irradiation wavelength between 442 and 365 nm. The absorbance changes at 398 nm (λ_{max}) were used to track the isomerization. (**C**) ^{1}H NMR spectra of **1**-*Z*,*Z*,*Z* and **1**-*E*,*E*,*E* (1.0 mM in CD_2Cl_2) before (0 equiv) and after titrating with 1 equiv of TBACl. eq, equivalent. (**D**) Job's plot analysis of the complexation between **1**-*E*,*E*,*E* and TBACl in CD_2Cl_2 at 298 K.

photoisomerization process can be cycled multiple times (10 cycles observed) with no obvious signs of fatigue (Fig. 2B). The thermal *E*→*Z* isomerization at 298 K is extremely slow, and only ~0.4% change in the isomer ratio is observed after a month (fig. S22).

Binding affinity

The binding affinity of **1**-*E* (97% *E*; 1.0 mM) with anions in CD_2Cl_2 was first studied by use of NMR spectroscopy (Fig. 2C). Throughout the titration experiments, only one set of shifting ^{1}H NMR signals was observed, indicating that the three hydrazone units in **1** contribute equally to the process—it is not stepwise, at least on the NMR timescale. In general, and upon titration (figs. S43, S47, and S51) of the *E*-rich solution of **1** with the *t*-butyl-ammonium salt of the halogen anions (TBAX), the triazolyl CH (H2) and hydrazone NH protons exhibited the most substantial downfield chemical shifts [for example, for Cl^-, the shifts are from 8.33 to 9.04 parts per million (ppm) and 8.57 to 9.10 ppm, respectively]. This observation indicates that the polarized triazolyl C–H and hydrazone N–H protons are the primary binding sites for the anionic guests. The other protons (such as H3, H4, H5, and H6) have less obvious shifts, which implies that these protons have weaker contributions to the binding event. In general, the shift is greater for the smaller halogens ($Cl^- > Br^- > I^-$), indicating that the binding is following suit as well. As for the bulkier anions, BF_4^- and PF_6^-, the triazolyl CH proton barely shifts, whereas the hydrazone NH proton undergoes an obvious downfield shift, indicating a weaker binding than with the halogens (figs. S55 and S57). We next characterized the anion binding properties of the *Z* isomer of **1** (Fig. 2C), and as expected, the formation of the intramolecular H bond with the carbonyl group precludes binding with the anions, and hence, we observed barely any up- or downfield shifts during the titrations (figs. S45, S49, and S53).

We next used Job's plot analysis to estimate the binding stoichiometry of receptor **1** with the halogen anions (where $K_2 \gg K_1$) (*46*), which yielded a 2:1 receptor-to-anion ratio (Fig. 2D). We were unsuccessful, even after many trials (tables S6 to S8), in obtaining single crystals of this complex that were suitable for x-ray crystallography analysis. Isothermal titration calorimetry (ITC) studies in 1,2-dichloroethane also revealed two binding events with high positive cooperativity (fig. S60) (*47*). Diffusion-ordered spectroscopy (DOSY) and negative electrospray ionization time-of-flight mass spectroscopy (TOF MS ES$^-$) also lent evidence for the 2:1 complexation, and DOSY experiments support the positive cooperativity aspect of the binding events (2:1 dominates at low Cl^- concentration, whereas a high concentration pushes toward a 1:1 complex). In the DOSY analyses, a 10.0-mM solution of free *E* receptor exhibits a diffusion coefficient (*D*) of 6.58×10^{-6} cm^2 s^{-1} (figs. S28A and S29). With the addition of 0.5 equiv of Cl^-, we observed a dominant 2:1 complex with a diffusion constant of 4.79×10^{-6} cm^2 S^{-1}, which is larger than the unbound receptor (figs. S28B and S30). As the Cl^- concentration was increased from 2.4 to 10 equiv, the population of the smaller complex ($D = 9.00 \times 10^{-6}$ cm^2 s^{-1}), presumed to be the 1:1 complex, increased and eventually became the dominant species in

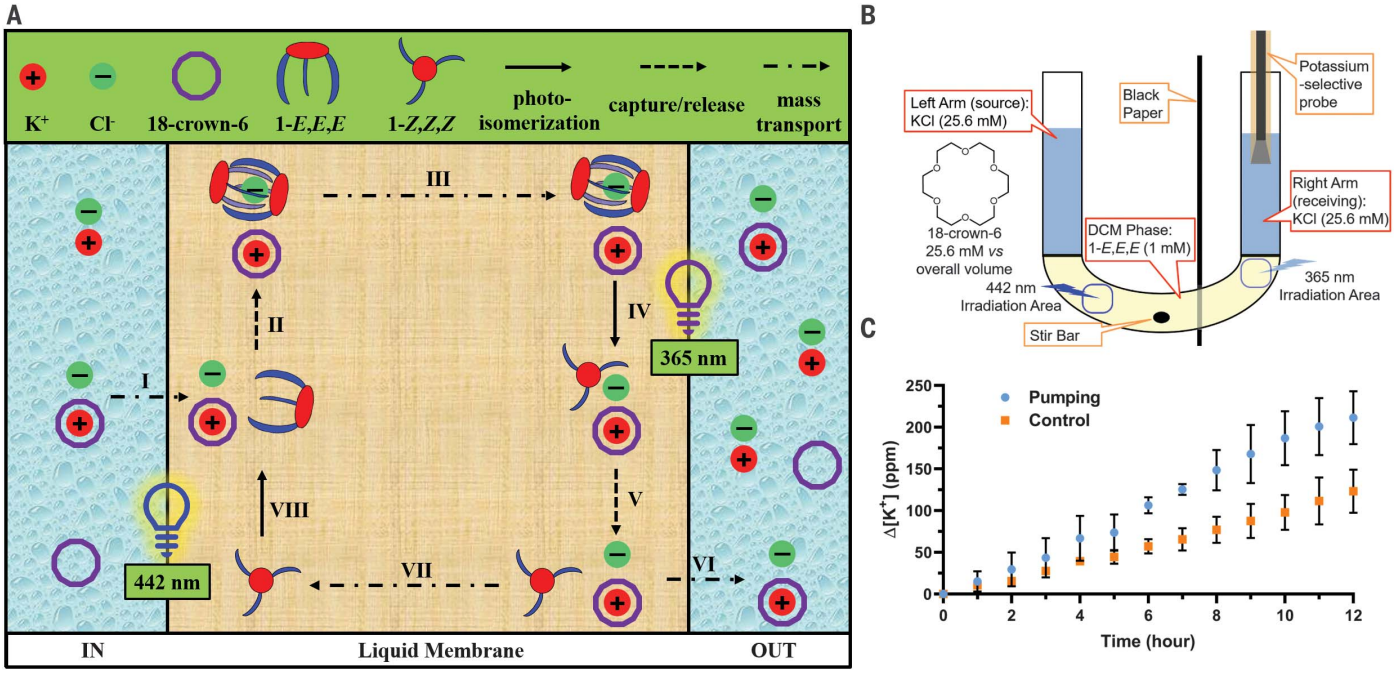

Fig. 3. Pumping anions against a concentration gradient. (**A**) Top-down graphic of the U-tube illustrating the pumping of the KCl ion pair though the DCM liquid membrane; all the chemicals involved as well as the pumping pathways are denoted. (**B**) Details of the U-tube experimental setup, in which the left (source) and right (receiving) arm are equipped with 1000-ppm KCl solution and separated by a DCM liquid membrane containing **1**-*E*,*E*,*E* (1.0 mM), 18-crown-6 (to facilitate the transport of the counter cation), and a potassium-selective probe (to measure the potassium concentration in the receiving phase over time). (**C**) Potassium concentration (in ppm) at the receiving (OUT) phase monitored as a function of time; the blue dots represent the pumping results (N = 3), and the orange dots represent the control experiment without the participation of **1**-*E*,*E*,*E* (N = 3); error bars indicate the standard deviation; the net pumping capability of this system is 8.8% over 12 hours.

solution (figs. S28, C and D; S31; and S32). The volume ratios, derived from the Stokes-Einstein relationship, gave $V_{Cl^-\ 2:1}/V_{free}$ = 2.6 and $V_{Cl^-\ 1:1}/V_{free}$ = 0.4 (Eqs. S11 to S13), indicating that the 2:1 complex is 2.6 times larger than the unbound receptor, whereas the 1:1 complex is about half the size, indicating that the molecule becomes more compact upon coordination with a Cl^- ion. By contrast, introducing $TBABF_4$ (30.0 equiv) or $TBAPF_6$ (50.0 equiv) to the *E* isomer (1.0 mM) increased the diffusion coefficient to 1.23×10^{-5} $cm^2\ s^{-1}$ and 1.23×10^{-5} $cm^2\ s^{-1}$ (figs. S34 and S35), respectively, indicating the formation of even smaller particles. These results further support that hydrazone **1**-*E*,*E*,*E* forms a 2:1 complex with smaller halide anions and a 1:1 complex with larger ones, which is in alignment with the data obtained from the Job's plot (figs. S23 to S27). The latter outcome can be attributed to a geometrical mismatch between the trimer and these bulkier anions, which results in substantially lower binding constants, even with the *E* isomer (Table 1).

TOF MS ES^- experiments were conducted on a sample composed primarily of the *E* isomer (>95%, according to NMR spectroscopy), and a mass of 2421.7617 u was measured, which is the expected mass (calc. is 2421.7623 u) for a 2:1 complex between two *E* isomers and a Cl^- anion. This conclusion is strongly supported by the isotope distribution, which seamlessly aligns with the chemical formula of the 2:1 complex (fig. S37). A 1:1 complex (calc. 1228.3659) with a mass of 1228.3654 u was also observed in the same solution, and its identity was confirmed with isotope and elemental composition analyses (figs. S39 and S40). A *Z*-rich sample only showed the signal of the pure hydrazone [mass/charge ratio (m/z) = 1194.4048 u, cal. 1194.4038 u in positive ion mode; and m/z = 1192.3872 u, cal. 1192.3891 u in negative ion mode] (fig. S42); no complex was formed with the Cl^-. In the case of PF_6^-, only the mass of the 1:1 complex was observed with the *E* isomer (m/z = 1338.3654 u, cal. 1338.3612 u) (fig. S41), which matches the Job's plot results (fig. S27).

Fitting the ^1H NMR titration results for Cl^- with the *E* isomer by using a 2:1 binding model in *HypNMR2008* resulted in an overall binding constant (β_2) of 2.05 ± 0.14 × 10^6 M^{-2} (Table 1 and fig. S44). A similar binding constant was also obtained in the ITC studies in 1,2-dichloroethane (fig. S60). When the ion pairing is taken into consideration, the net binding constant between Cl^- and hydrazone **1**-*E*,*E*,*E* in DCM increases to 10^{11} M^{-2} (fig. S59 and eqs. S14 to S17) (*48*–*50*). Fitting the ^1H NMR titration results of Cl^- with the *Z* isomer by using a 1:1 model yields a binding affinity of 9 ± 1 M^{-1} ($10^{5.6}$ M^{-1} when ion pairing is considered), indicating the low binding affinity of the *Z* isomer with Cl^-. This tremendous decrease in binding strength [up to six orders of magnitude, whereas the affinity difference of the next most effective receptor is four orders of magnitude (*28*)] highlights the crucial contribution of the NH protons to the anion binding properties of receptor **1** (unlike other systems, the triazolyl CH proton is not playing a major role in the binding). We observed a similar trend for the other two halogen anions (Table 1). Overall, these results show that switching hydrazone **1** between its *Z* and *E* isomers by use of light allows for efficient control over the halogen anion binding affinity of the receptor.

Application to chloride transport

We next took advantage of the excellent photoswitching properties of the receptor and the huge difference in binding affinity upon photoswitching to pump Cl^- (which gave a slightly larger binding difference than did Br^-) through a liquid membrane against a concentration gradient (Fig. 3, A and B). We decided to use a U-tube for compartmentalization instead of a membrane, which is what biology studies use to control over species concentrations (*1*, *51*). To this end, we introduced a KCl (25.6 mM, 1000 ppm K^+) aqueous solution at both the anion feedstock

(IN phase) and the receiving phase (OUT phase). The two phases were separated by a DCM phase containing **1**-*E* (1.0 mM). 18-crown-6 (25.6 mM) was introduced and evenly distributed in all phases to assist the transportation of counter cation (K^+) (Fig. 3A, processes I and VI) (*52*). A stir bar was placed in the DCM phase, and the stirring speed was set to 100 rotations per minute (rpm). The 442-nm light source (Andover bandpass filter 442F5X10-25 with a HBW of 10 nm) was positioned close to the interface between the IN and DCM phases to maintain an *E*-rich environment at that region (Fig. 3A, process VIII). A 365-nm-wavelength light source (DARKBEAM 365 SK68 UV Flashlight) (supplementary materials) was positioned close to the interface between the DCM and OUT phases to switch the receptors to the *Z* form (Fig. 3A, process IV) and hence facilitate the release of the anions from liquid membrane to the receiving aqueous phase (Fig. 3A, processes V and VI). Subsequently, we used a potassium-selective probe to measure the concentration of K^+ over time in the OUT phase to assess the concentration change in Cl^-. After 12 hours of continuous operation, the concentration in the receiving phase increased by 211.4 ± 25.9 ppm (table S3), according to three consecutive measurements. We conducted control experiments with the same setup but in the absence of **1** to elaborate on this finding. The results of the control showed that after 12 hours, the concentration of the OUT phase increased by 123.2 ± 21.1 ppm, which we attributed to the evaporation of water. After taking this evaporation-induced concentration rise into account, the pumping system demonstrated an active transport of 8.8 ± 2.6% Cl^- against the concentration gradient in 12 hours (Fig. 3C), which corresponds to a membrane potential of 4.2 mV being built up (supplementary materials, section 14). The distance the Cl^- ion is being transported is ~3.5 cm (equivalent to kicking a soccer ball the length of 65,000 football fields), which shows the ability of this system to function at large scales. After the pumping, and facilitated by the crown ether, the system undergoes a slow reequilibration process under dark (fig. S63).

To study the role of stirring in this pumping process, we conducted a control experiment (fig. S62) in which we repeated the measurements without stirring the solution. After 12 hours of operation, the K^+ concentration in the OUT phase increased by 108.0 ppm through evaporation (table S3, column 3). This increase is consistent with another control experiment that omitted the hydrazone from the mixture and underscores the necessity of stirring in facilitating mass transport. To qualitatively assess and mitigate the influence of evaporation, we further modified our experimental setup. Instead of using a probe, we sealed both sides of the U-tube with parafilm while keeping all the other parameters constant (1.0 mM of **1**-*E* in DCM with a stir bar operating at a 100-rpm stirring rate, 25.6 mM 18-crown-6 distributed throughout the solutions, and two beams of light at the interfaces) (fig. S61E). Samples were collected before and after the irradiation and analyzed by inductively coupled plasma mass spectrometry (ICP-MS). The initial K^+ concentration was measured as 900.5 ± 42.0 ppm. After 12 hours, the concentration in the IN phase was reduced to 870.8 ± 8.0 ppm, whereas the OUT phase increased to 937.3 ± 8.0 ppm (table S4). These results again confirm that transport against a gradient is occurring. In this instance, 4.1% of Cl^- ion is being transported against the gradient. The discrepancy between the two results most likely results from the different setups used in the experiments. On the basis of these experiments, the operational yield of our anion pump was determined to be 4.1 to 8.8%, which is comparable with those of other molecular pumps reported in the literature (table S5). The distance (3.5 cm) at which our system is operating is substantially greater. Nonetheless, the operation of the porphyrin-based membrane pump (*39*) is far more efficient (although the transport distance, 120 nm, is much smaller), which is expected from a system that relies on bulk effects versus one in which molecular machines are actively transporting the anions from one end to another.

We developed a hydrazone-based photoswitchable anion receptor and used it in the efficient capture and release of anions. The *E* isomer of the switch exhibits superior binding affinity to halide ions (Cl^-, Br^-, and I^-) compared with bulkier anions (BF_4^- and PF_6^-). Switching to the intramolecularly H-bonded *Z* configuration substantially diminishes the binding ability of the receptor (up to six orders of magnitude), despite the presence of three electron-deficient triazole rings in the system. The dual functionality of the trimeric hydrazone **1**, serving as both the anion binder and the binding photomodulator, offers a straightforward strategy for actively pumping KCl across a solvent membrane. This pumping process results in a 4.1 to 8.8% transfer of Cl^- against a gradient in a 12-hour period.

REFERENCES AND NOTES

1. D. C. Gadsby, *Nat. Rev. Mol. Cell Biol.* **10**, 344–352 (2009).
2. J. M. Russell, *Physiol. Rev.* **80**, 211–276 (2000).
3. S. M. O'Grady, H. C. Palfrey, M. Field, *Am. J. Physiol.* **253**, C177–C192 (1987).
4. G. Jiang *et al*., *Am. J. Physiol. Heart Circ. Physiol.* **286**, H1552–H1557 (2004).
5. E. K. Hoffmann, P. B. Dunham, in *International Review of Cytology*, vol. 161, K. W. Jeon, J. Jarvik, Eds. (Elsevier, 1995), pp. 173–262.
6. M. Haas, *Am. J. Physiol.* **267**, C869–C885 (1994).
7. V. I. Dzhala *et al*., *Nat. Med.* **11**, 1205–1213 (2005).
8. M. A. Shannon *et al*., *Nature* **452**, 301–310 (2008).
9. N. Kaltsoyannis, S. T. Liddle, *Chem* **1**, 659–662 (2016).
10. Y. Qiu *et al*., *Science* **368**, 1247–1253 (2020).
11. S. Amano, S. D. P. Fielden, D. A. Leigh, *Nature* **594**, 529–534 (2021).
12. L. Feng *et al*., *Science* **374**, 1215–1221 (2021).
13. S. Corra *et al*., *Nat. Nanotechnol.* **17**, 746–751 (2022).
14. J. F. Stoddart, *Angew. Chem. Int. Ed.* **56**, 11094–11125 (2017).
15. Y. Qiu, Y. Feng, Q.-H. Guo, R. D. Astumian, J. F. Stoddart, *Chem* **6**, 1952–1977 (2020).
16. J. T. Davis, P. A. Gale, R. Quesada, *Chem. Soc. Rev.* **49**, 6056–6086 (2020).
17. J. de Jong, J. E. Bos, S. J. Wezenberg, *Chem. Rev.* **123**, 8530–8574 (2023).
18. D. A. McNaughton *et al*., *Chem* **9**, 3045–3112 (2023).
19. T. G. Johnson, M. J. Langton, *J. Am. Chem. Soc.* **145**, 27167–27184 (2023).
20. L. K. Macreadie *et al*., *Chem* **8**, 46–118 (2022).
21. J. Pancholi, P. D. Beer, *Coord. Chem. Rev.* **416**, 213281 (2020).
22. D. Villarón, S. J. Wezenberg, *Angew. Chem. Int. Ed.* **59**, 13192–13202 (2020).
23. Y. Hua, A. H. Flood, *J. Am. Chem. Soc.* **132**, 12838–12840 (2010).
24. F. C. Parks *et al*., *J. Am. Chem. Soc.* **140**, 17711–17723 (2018).
25. S. J. Wezenberg, M. Vlatković, J. C. M. Kistemaker, B. L. Feringa, *J. Am. Chem. Soc.* **136**, 16784–16787 (2014).
26. Z. Kokan, M. J. Chmielewski, *J. Am. Chem. Soc.* **140**, 16010–16014 (2018).
27. P. Molina, F. Zapata, A. Caballero, *Chem. Rev.* **117**, 9907–9972 (2017).
28. D. Villarón, M. A. Siegler, S. J. Wezenberg, *Chem. Sci.* **12**, 3188–3193 (2021).
29. G. Steinberg-Yfrach *et al*., *Nature* **385**, 239–241 (1997).
30. I. M. Bennett *et al*., *Nature* **420**, 398–401 (2002).
31. X. Xie, G. A. Crespo, G. Mistlberger, E. Bakker, *Nat. Chem.* **6**, 202–207 (2014).
32. P. D. Beer, P. A. Gale, *Angew. Chem. Int. Ed.* **40**, 486–516 (2001).
33. Y. Liu, W. Zhao, C.-H. Chen, A. H. Flood, *Science* **365**, 159–161 (2019).
34. A. Kerckhoffs, M. J. Langton, *Chem. Sci.* **11**, 6325–6331 (2020).
35. N. Busschaert *et al*., *Nat. Chem.* **9**, 667–675 (2017).
36. S. J. Wezenberg *et al*., *J. Am. Chem. Soc.* **144**, 331–338 (2022).
37. D. S. Kim, J. L. Sessler, *Chem. Soc. Rev.* **44**, 532–546 (2015).
38. S. Shinkai, T. Nakaji, T. Ogawa, K. Shigematsu, O. Manabe, *J. Am. Chem. Soc.* **103**, 111–115 (1981).
39. C. Li *et al*., *Nat. Commun.* **15**, 832 (2024).
40. X. Su, I. Aprahamian, *Chem. Soc. Rev.* **43**, 1963–1981 (2014).
41. B. Shao, I. Aprahamian, *Chem* **6**, 2162–2173 (2020).
42. J. Filo *et al*., *RSC Adv.* **9**, 15910–15916 (2019).
43. B. Shao, H. Qian, Q. Li, I. Aprahamian, *J. Am. Chem. Soc.* **141**, 8364–8371 (2019).
44. I. Aprahamian, *ACS Cent. Sci.* **6**, 347–358 (2020).
45. In the presence of 10 equiv of Cl^- anions, the quantum yield was determined to be $\Phi_{Z\rightarrow E}$ = 4.9 ± 0.1% (fig. S20) and $\Phi_{E\rightarrow Z}$ = 4.5 ± 0.1% (fig. S21), showing that binding with the anion is not changing the photoswitching process.
46. D. B. Hibbert, P. Thordarson, *Chem. Commun.* **52**, 12792–12805 (2016).
47. DCM has a low boiling point that is not compatible with the long periods of time required for ITC measurements.
48. Y. Liu, A. Sengupta, K. Raghavachari, A. H. Flood, *Chem* **3**, 411–427 (2017).
49. R. O. Ramabhadran *et al*., *J. Am. Chem. Soc.* **136**, 5078–5089 (2014).
50. S. Alunni, A. Pero, G. Reichenbach, *J. Chem. Soc., Perkin Trans. 2* (8): 1747–1750 (1998).
51. A. D. Gruia, A.-N. Bondar, J. C. Smith, S. Fischer, *Structure* **13**, 617–627 (2005).
52. When pumping Cl^- in the presence of crown ether, ion pairing competition could be compromised, which would lead to a higher net binding affinity and thus a better pumping performance.

ACKNOWLEDGMENTS

We thank B.-N. T. Nguyen (Stanford University) and A. B. Grommet (Chalmers University of Technology) for helpful advice about the U-shaped tube experiments; M. Pellegrini for the 2D ROESY NMR studies; and B. Jackson for ICP-MS analyses. **Funding:**

This work was supported by the NSF (CHE-2304983). The Dartmouth Trace Element Analysis Core Facility is supported by the Dartmouth Cancer Center with NCI Cancer Center Support Grant 5P30CA023108. **Author contributions:** B.S. designed and synthesized the molecule and conducted the UV/Vis spectroscopy studies; H.F. performed NMR titration experiments, Job's plot, DOSY, and U-shaped tube experiments. Both B.S. and H.F. analyzed the results, under the supervision of I.A. The manuscript was drafted jointly by B.S., H.F., and I.A., and all authors commented on and approved the manuscript. **Competing interests:** The authors declare no conflicts of interest. **Data and materials availability:** All the data needed to understand and assess the conclusions are available in the main text and supplementary materials.

SUPPLEMENTARY MATERIALS

science.org/doi/10.1126/science.adp3506
Materials and Methods
Figs. S1 to S63
Tables S1 to S8
References (*53*–*57*)

Submitted 20 March 2024; accepted 2 July 2024
10.1126/science.adp3506